The Astrophysical Journal, 906:55 (8pp), 2021 January 1 https://doi.org/10.3847/1538-4357/abc87b

Detection of PO in Orion-KL: Phosphorus Chemistry in the Plateau Outflow

J. J. Bernal[1], L. A. Koelemay[1], and L. M. Ziurys[1,2]
[1] Department of Chemistry and Biochemistry, University of Arizona, Tucson, AZ 85721, USA
[2] Department of Astronomy, Steward Observatory, University of Arizona, 933 North Cherry Ave., Tucson, AZ 85721, USA
Received 2020 September 16; revised 2020 October 23; accepted 2020 November 6; published 2021 January 7

Abstract

The PO molecule ($X^2\Pi_r$) has been detected toward Orion-KL via its $J = 2.5 \rightarrow 1.5$ transition near 109 GHz using the 12 m telescope of the Arizona Radio Observatory. This transition consists of a quartet of lines, generated by lambda-doubling and phosphorus hyperfine interactions, creating a distinct pattern of doublets of doublets. All four features ($F = 3 \rightarrow 2$, *e, f* and $2 \rightarrow 1$, *e, f*) were detected. The line profiles measured were relatively broad, with $\Delta V_{1/2} \sim 21$–25 km s^{-1}, and $V_{\rm LSR} \sim 10$ km s^{-1}, clearly identifying the molecule as arising from the Orion "plateau" region. The $J = 2 \rightarrow 1$ transition of PN ($X^1\Sigma$) at 94 GHz was also measured, and its line profile indicates a plateau origin in Orion, as found previously by Ziurys. Therefore, PO and PN arise from the same gas. There was no evidence of a "hot core" or "ridge" component in either molecule. The column densities determined for PO and PN in the Orion plateau are $N_{\rm tot} \approx 5.4(0.2) \times 10^{13}$ and $2.0(0.4) \times 10^{13}$ cm^{-2}, respectively, with corresponding abundances, relative to H_2, of $f \sim 1.6(0.1) \times 10^{-10}$ and $6.1(0.6) \times 10^{-11}$, resulting in PO/PN ~ 3. The PO and PN line profiles also resemble those of SiO and SiS, suggesting that the phosphorus molecules are produced by shocks in the plateau outflow. The observed PO/PN ratio in Orion-KL is very close in value to that measured in other warm molecular clouds, indicating a common synthesis pathway for these two molecules in outflows caused by star formation.

Unified Astronomy Thesaurus concepts: Astrochemistry (75); Star formation (1569); Interstellar abundances (832); Interstellar molecules (849); Molecular clouds (1072); Astrobiology (74)

1. Introduction

Phosphorus clearly plays a central role in astrobiology. It is the fifth most abundant element in living systems by mass after C, N, O, and H (e.g., Maciá 2005), and is important for replication, metabolism, and cellular structure. For example, phosphate esters create the backbone of deoxyribonucleic acid (DNA) and ribonucleic acid (RNA). The widespread presence in the Earth's current biosphere of related catalysts and cofactors suggests that RNA may have been the first biopolymer. Furthermore, adenosine triphosphate or ATP, the key molecule in the cell energy cycle, has three phosphate ester groups containing P–O bonds that store and release energy for this process. A phosphate ester is also found in phospholipids, which are the main structural components of cellular membranes in living systems (Harayama & Riezman 2018).

In addition to its biological importance, phosphorus is significant in solar system materials. Apatite, $Ca_5(PO_4)_3(OH, F, Cl)$, for example, is widely distributed in planetary bodies, and is known to trap volatiles such as chlorine, sulfur, and water (e.g., Hughes & Rakovan 2002; Barnes et al. 2014). Phosphorus has been additionally found in the coma of comets, for example, in 67P/Churyumov–Gerasimenko (Altwegg et al. 2016; Rivilla et al. 2020), suggesting the element also exists in the comet nucleus. In meteorites, phosphorus occurs as a major solute in the phosphide schreibersite, $(Fe,Ni)P_3$, or as part of a polyatomic anion in phosphates (PO_4^{3-} bonded with Ca^{2+}, Mg^{2+}, etc., Pasek 2019). PH_3, phosphine, has also been identified in the gas phase in the atmospheres of Jupiter and Saturn (e.g., Fletcher et al. 2009).

In the interstellar medium (ISM), phosphorus has been more elusive. Many of its atomic transitions are not easily accessed by ground-based telescopes (e.g., Jacobsen et al. 2014) Observations toward diffuse clouds of P II lines suggest that the element is not very depleted, despite its refractory nature (Lebouteiller et al. 2006). More recently, measurements of PI fine structure multiplet in the infrared have shown it to be abundant near certain supernovae (SN) remnants (e.g., Koo et al. 2013), providing strong evidence of an origin in oxygen and neon-shell burning in Type II SN. In addition to gas-phase carriers, thermodynamics predicts that phosphorus in the solid state should be condensed into the dust grains as the mineral schreibersite (e.g., Lodders & Fegley 1999; Lodders 2003).

Molecules have also provided an avenue to study the distribution of phosphorus in the colder ISM. The first detection of an interstellar P-bearing species was in 1987, when Ziurys observed PN in the Orion-KL region. The broad line profile measured in this work identified the presence of this species in the so-called "plateau" outflow of Orion. PN was subsequently observed in additional sources, including massive dense or cold cloud cores (e.g., Turner et al. 1990; Fontani et al. 2016). It remained for many years the only phosphorus-containing molecule identified in dense clouds. In contrast, circumstellar envelopes were found to contain a variety of P-bearing species, starting with the detection of CP in the shell of the carbon-rich star, IRC+10216 (Guélin et al. 1990). This identification was followed by the detections of PN, CCP, HCP, and PH_3 in IRC+10216 (e.g., Agúndez et al. 2007, 2008, 2014; Halfen et al. 2008; Milam et al. 2008; Tenenbaum & Ziurys 2008), as well as PO and PN in the O-rich shell of the supergiant star VY Canis Majoris (Tenenbaum et al. 2007; Milam et al. 2008). Very recently, PO and PN have been observed in other O-rich circumstellar shells (de Beck et al. 2013; Ziurys et al. 2018). The observation of PO was particularly interesting, as this was the first molecule observed in space with a phosphorus–oxygen bond.

A recent breakthrough in interstellar phosphorus chemistry has been the detections of PO in star-forming molecular clouds.

In 2016, Rivilla et al. identified PO in the high-mass star-forming regions W51 1e/2e and W3(OH), along with PN. These authors suggested that both molecules are related and arose from gas-phase chemistry in core collapse, followed by evaporation in the young star phase. Shortly thereafter, Lefloch et al. (2016) observed PO, along with PN, in the low mass star-forming region L1157. Because PN appeared to be associated with SiO, these authors attributed the formation of the phosphorus-bearing molecules to shocks. PO and PN were subsequently identified in the star-forming regions G + 0.693 −0.03 and AFGL 5142 (Rivilla et al. 2018, 2020), as well as the low mass protostar B1 (Bergner et al. 2019). Again, shock-related chemistries were thought to account for the synthesis of these molecules in two of these sources, while in AFGL 5142, photochemistry was invoked. In addition, Fontani et al. (2016) discovered new sources of PN in massive dense cloud cores. Overall, the observations suggest that the formation mechanisms of PO and PN are related, but can be created under both quiescent and energetic conditions.

Here we report the detection of PO toward yet another star-forming region, Orion-KL. Orion-KL is a particularly good source to examine the chemistry of phosphorus. It is well-studied and relatively close in distance (437 ± 19 pc: Hirota et al. 2007); furthermore, it contains distinct kinematic regions, visible within a given line profile, with known physical properties. PO was identified in Orion-KL by its four hyperfine components of the lambda-doublets of the $J = 2.5 \rightarrow 1.5$ transition near 109 GHz, using the 12 m telescope of the Arizona Radio Observatory (ARO). A tentative detection of PO in Orion-KL had been reported previously by Ziurys (1988). The PO line profile was broad ($\sim$20 km s^{-1}), indicating that it arises from the plateau outflow, similar to PN. In this paper we present our observations and analysis, and the implications of the results for the chemistry of interstellar phosphorus.

2. Observations

The observations were conducted during the period 2016 March to 2017 November using the ARO 12 m on Kitt Peak, Arizona. The PO and PN measurements were acquired in the course of a 3 mm spectral survey toward Orion-KL (J. J. Bernal et al. 2020, in preparation). The survey observations covered a frequency range of 83.960–116.048 GHz. A dual polarization, 3 mm receiver comprised of ALMA Band 3, sideband separating mixers was used for observations (e.g., Freund et al. 2011). The backend used was a Millimeter Auto Correlator (MAC) with 195 kHz frequency resolution and with 600 MHz instantaneous, continuous bandwidth, for each receiver polarization. Typical image rejection, intrinsic in the mixer architecture, was $\sim$20 dB. The intensity scale was determined by the chopper wheel method, measured in units of T_A^* (K). The radiation temperature is then $T_R = T_A^*/\eta_b$, where η_b is the main beam efficiency: at 109 GHz, $\eta_b \sim 0.85$. System temperatures during observations were typically <150 K, with typical rms (1σ) noise levels of 3 mK at 195 kHz resolution. The beam size of the ARO 12 m antenna is $\theta_b \sim 58''$ at 109 GHz.

Observations were conducted in position-switching mode, with the off position 30′ W in azimuth. Telescope pointing was monitored on strong continuum sources such as Venus. Local oscillator shifts were performed to check for image contamination. Survey data were taken such that there was a $\sim$100 MHz overlap between observed frequencies. The data was smoothed from 195 kHz (0.54 km s^{-1}) to 1 MHz resolution (2.8 km s^{-1}) for all measured spectra, sufficient for Orion-KL where linewidths typically are 4–25 km s^{-1} (e.g., Tercero et al. 2010). Integration times are 20 and 5 hr for the frequency tunings 108.750 and 109.250 GHz, respectively, and 12, 11, and 6.5 hr at 93.750 GHz (PN), 84.750 GHz (^{30}SiO), and 90.750 GHz (SiS). Besides PO and PN, the data set included the frequencies of 3 mm transitions of CP and CCP.

3. Results

The spectra observed for the $J = 2.5 \rightarrow 1.5$ transition of PO are shown in Figure 1. The two lambda doublets that comprise this transition, labeled *e* and *f*, and each consisting of two phosphorus hyperfine components $F = 3 \rightarrow 2$ and $F = 2 \rightarrow 1$, were detected. The $F = 3 \rightarrow 2$ lines are indicated in red and the $F = 2 \rightarrow 1$ features in blue, respectively. The two *e* doublet lines were observed in two different frequency settings, 108.750 and 109.250 GHz. Although the observed lines are relatively weak ($T_A^* \sim$ 10–20 mK), the signal-to-noise is good (10–15). The $F = 3 \rightarrow 2$ features appear to be stronger than the $F = 2 \rightarrow 1$ counterparts by near the expected theoretical intensity ratio of 1:0.6. As is also evident from the figure, the $F = 2 \rightarrow 1$ *f* component of PO lies in the wing of the $N = 3 \rightarrow 2$, $J = 2 \rightarrow 1$ transition of SO, but is clearly distinguishable. The $F = 3 \rightarrow 2$ *f* transition may be partially blended with the $J_{Ka,Kc} = 16_{1,15} \rightarrow 15_{1,14}$ line of gauche ethyl formate (e.g., Rivilla et al. 2016). However, the $J_{Ka,Kc} = 16_{2,15} \rightarrow 15_{2,14}$ and the $J_{Ka,Kc} = 15_{1,14} \rightarrow 14_{1,13}$ transitions of this molecule, which have intensities very similar to the potential contaminating line, were not detected to a noise level of 7 mK, peak-to-peak. Therefore, the contribution of ethyl formate to the overall intensity of the PO lines is likely to be <10 %. Unlike Rivilla et al. (2016), we found also little evidence for contamination of the $F = 2 \rightarrow 1$ *f* component of PO by the $J_{Ka,Kc} = 10_{8,2} \rightarrow 9_{8,1}$ and $J_{Ka,Kc} = 10_{9,1} \rightarrow 9_{9,0}$ ($v = 1$–0, aGg' conformer) transitions of ethylene glycol, which lie 2 MHz away in frequency, or 5 km s^{-1}. The $J_{Ka,Kc} = 11_{0,11} \rightarrow 10_{0,10}$ transition of this conformer (111.841 GHz) was not detected in the survey to a level of <6 mK. The $J_{Ka,Kc} = 11_{0,11} \rightarrow 10_{0,10}$ line lies lower in energy than the possible contaminating features by >19 cm^{-1} and is a factor of 3.6 stronger than their combined intensity. The estimated contribution to the $F = 2 \rightarrow 1$ *f* component of PO by ethylene glycol is therefore <2 mK (or <18%), well within the uncertainties.

A spectrum of the $J = 2 \rightarrow 1$ transition of PN near 94 GHz in Orion-KL is presented in Figure 2 (upper panel). This line had been previously observed by Ziurys (1987), and the line profile is identical, given the respective noise levels, with an intensity near 20 mK. For comparison, the $J = 2 \rightarrow 1$ transition of ^{30}SiO near 84 GHz is also shown in the figure (lower panel). This less abundant isotopologue of SiO was chosen to avoid the effects of high opacity. The ^{30}SiO line is partially contaminated ($\sim$28% of the line intensity) by the $J\tau = 19_4 \rightarrow 18_5$ transition of CH_3OH, which lies to lower frequency, as noted by Ziurys (1988). A Gaussian fit to the line profile of ^{30}SiO is shown on the spectrum in red. Although SiO also exhibits the high-velocity wings that trace the SE-NW outflow seen in vibrationally excited H_2 (e.g., Feng et al. 2015), the bulk of the emission appears to arise from the plateau component (e.g., Tercero et al. 2011). The PN and SiO line

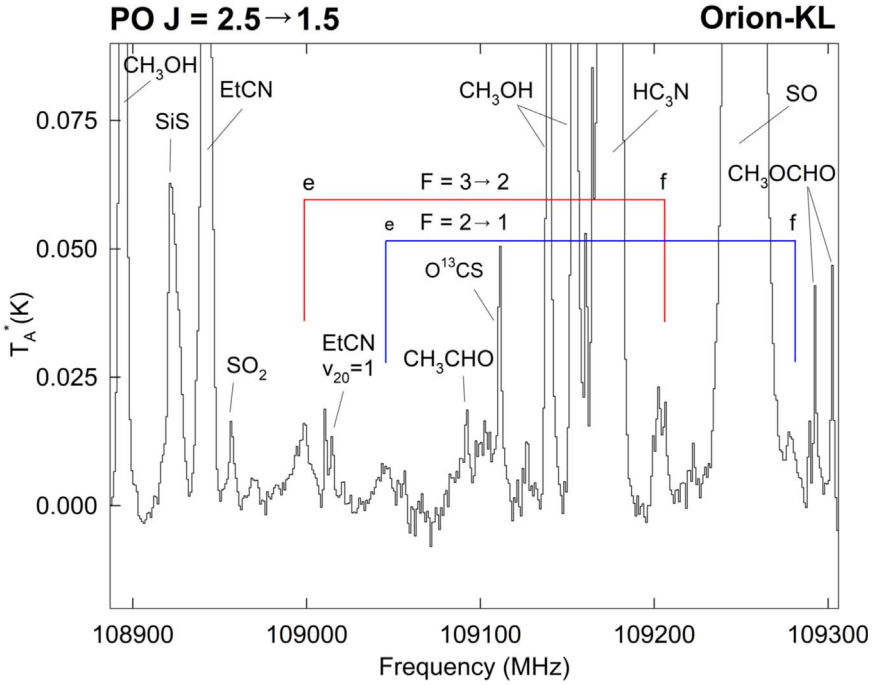

Figure 1. Spectra of the $J = 2.5 \rightarrow 1.5$ transition of PO observed toward Orion-KL with the ARO 12 m telescope. This transition consists of lambda doublets, labeled by *e* and *f*, each of which are further split into two hyperfine components, $F = 3 \rightarrow 2$ and $F = 2 \rightarrow 1$ (approximate relative intensity ratio 1:0.6), indicated by red and blue lines, respectively. All four lines are visible in the spectrum, except the $F = 2 \rightarrow 1$ *f* component appears in the line wing of the $N_J = 3_2 \rightarrow 2_1$ transition of SO. The broader line widths for PO indicate an origin in the Orion plateau. The spectrum was created from observations conducted at two frequencies, 108.750 and 109.250 GHz, and then combined. All data were taken with 195 kHz frequency resolution and then smoothed to 1 MHz.

profiles are very similar, except that the high-velocity wings are not visible in the former molecule.

Figure 3 shows the $J = 5 \rightarrow 4$ and $J = 6 \rightarrow 5$ transitions of SiS observed in Orion-KL. SiS is thought to trace outflows and shocks, similar to SiO (Ziurys 1988, 1991). The line profiles of SiS resemble that of PN (Figure 1), linking these molecules to common, plateau gas. SiS does not show much evidence of the high-velocity line wings seen in the ^{30}SiO line profile.

No evidence was found in the data for CP and CCP. These molecules were not observed to upper limits of $T_A^* < 10$–12 mK, based on their $N = 2 \rightarrow 1$ and $J = 8.5 \rightarrow 7.5$ transitions, respectively.

Table 1 lists the measured intensities (T_A^*), LSR velocities, and linewidths $\Delta V_{1/2}$ for PO, PN, ^{30}SiO, and SiS derived from Gaussian fits to the line profiles. The fit to the ^{30}SiO spectrum excludes the high-velocity outflow and removes the contaminating CH_3OH feature. As is evident in the table, all spectra exhibit a velocity of $V_{LSR} \sim 9$–10 km s^{-1} with linewidths (FWHM) of $\Delta V_{1/2} \sim 20$–25 km s^{-1}, indicating a clear origin in the Orion plateau for the phosphorus and silicon species (e.g., see Tercero et al. 2010; Feng et al. 2015). Note that Tercero et al. (2010) estimated an FWHM linewidth of ~ 25 km s^{-1} for the plateau.

4. Analysis

To calculate column densities of PO and PN, the non-LTE radiative transfer code RADEX was used (van der Tak et al. 2007). Here line intensities T_R are modeled by adjusting the column density, based on a given gas kinetic temperature T_k and gas density $n(H_2)$. Because the data indicate that both molecules arise in the plateau, all spectra were corrected for beam dilution, assuming a source size of 30″ for the plateau (e.g., Tercero et al. 2010), and $\theta_b \sim 58''$–66″, depending on the frequency. Collisional rates for PO and PN were adapted from the BASECOL database (Dubernet et al. 2013). As described in detail by Ziurys et al. (2018), PN–H_2 rates were scaled from those of PN–He; the rates for PO–H_2 were mass-scaled from those of NO–H_2 (see Ziurys et al. 2018 for additional information). For the RADEX analysis, the kinetic temperature and gas density were held fixed to $T_K = 125$ K and $n(H_2) = 10^6$ cm^{-3} based on average values for the Orion plateau (Tercero et al. 2010). The column density was varied over the range of $N_{tot} \sim 1.0 \times 10^{11}$–$1.0 \times 10^{14}$ cm^{-2} for PO and PN, based on values observed for these molecules in other clouds. The step size used was 10% of the starting value across a decade range (for example, for the calculation range 1.0×10^{11}–1.0×10^{12}, a step size of 1.0×10^{10} was used). The best fit was determined by a reduced chi-square analysis. Fractional abundances, relative to H_2, were calculated using the hydrogen column density value of $N(H_2) = 3.3 \times 10^{23}$ cm^{-2} from Feng et al. (2015). (Note that Tercero et al. 2010 give a value of $N(H_2) = 2.1 \times 10^{23}$ cm^{-2}.) Resulting column densities $N_{tot}$and abundances f (X/H_2) for PO and PN in Orion are given in Table 2.

Upper limits were also calculated for CP and CCP. For CP, RADEX was used for the modeling, as per PO and PN, and collisional rates were adapted from those of the CN–H_2 system found in the LAMBDA database (Schöier et al. 2005), mass scaling in analogy to the NO–H_2 system for PO. The phosphorus hyperfine structure, separated by 2.4 MHz in the line used for the upper limit, was collapsed for the calculation. Modeling was done assuming a plateau and also an extended ridge component for CP. The plateau computation assumed the same parameters for PO and PN, with $\Delta V_{1/2} = 20$ km s^{-1}, while for the ridge, $T_K = 70$ K and $n(H_2) = 10^5$ cm^{-3} were assumed, with a linewidth of 4 km s^{-1} and a filling factor of 1

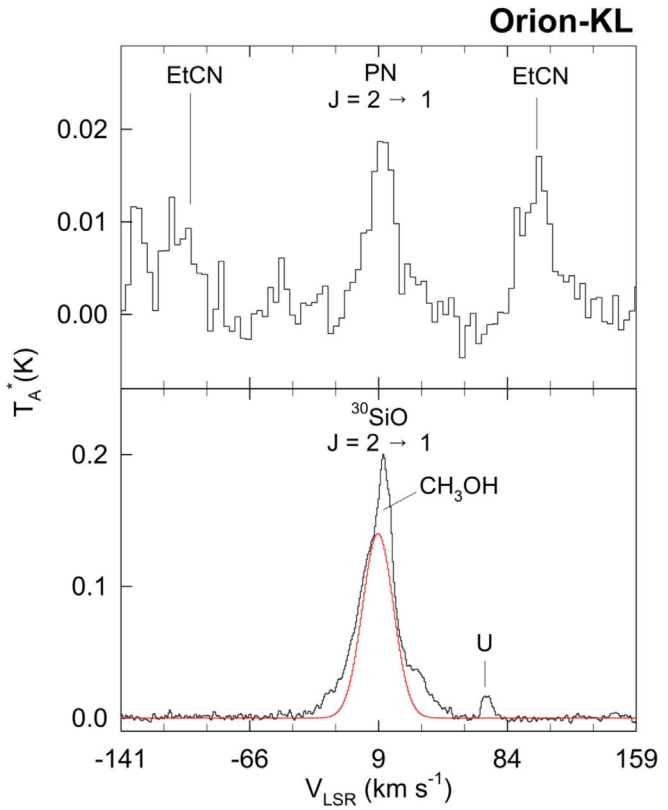

Figure 2. Spectrum of the $J = 2 \rightarrow 1$ transition of PN near 94 GHz observed toward Orion-KL with the ARO 12 m telescope (upper panel), as well as the $J = 2 \rightarrow 1$ line of ^{30}SiO at 84.746 GHz (lower panel). The SiO transition is partially blended with the $J\tau = 19_4 \rightarrow 18_5$ line of CH_3OH, which lies to lower frequency at 84.744 GHz (see Ziurys 1988). A Gaussian fit to the line profile (in red) indicates the SiO plateau component, which closely resembles the line shape for PN. The ^{30}SiO transition also exhibits high-velocity wings, which are not visible in PN. All data were taken with 195 kHz frequency resolution and then smoothed to 1 MHz.

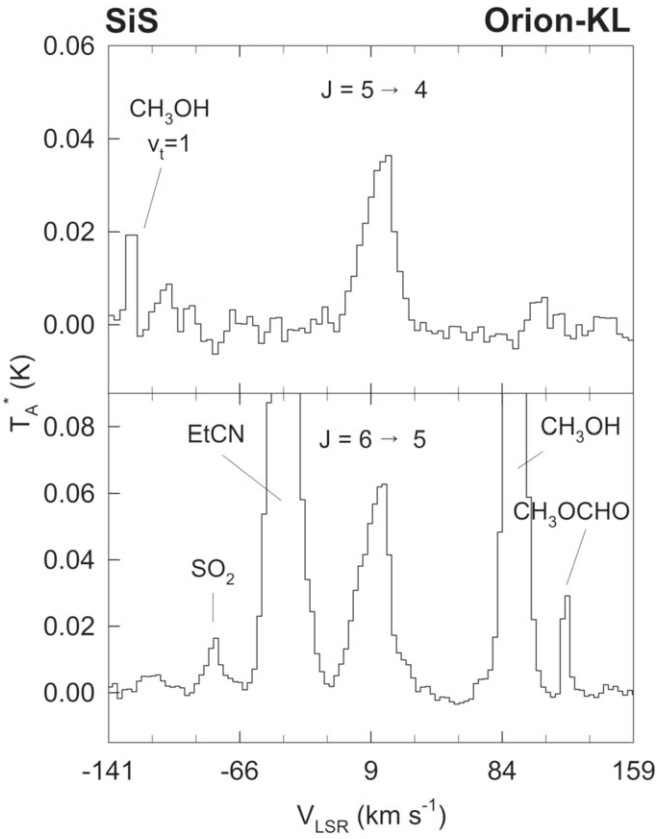

Figure 3. Spectra of the SiS $J = 5 \rightarrow 4$ and $J = 6 \rightarrow 5$ transitions near 90.7 and 108.9 GHz, respectively, observed toward Orion-KL with the ARO 12 m. The broad SiS line profiles suggest an origin in the Orion plateau, similar to PN and PO (see Table 1). All data were taken with 195 kHz frequency resolution and then smoothed to 1 MHz.

(see Tercero et al. 2010). Because it was difficult to find collisional rates that could be realistically adapted for CCP, upper limits for this molecule were calculated analytically for plateau and extended ridge sources, with the appropriate filling factor corrections, as described. A rotational temperature of 70 and 50 K were assumed for the plateau and ridge components, respectively, recognizing that $T_{rot} < T_K$ for high dipole moment molecules, with the linewidth used for CP, as described. CP upper limits were also calculated analytically as a confirmation of the RADEX results, and were found to be in excellent agreement, as shown in Table 3. Upper limits to the fractional abundances were derived using $N\ (H_2) = 3.3 \times 10^{23}\,cm^{-2}$ for the plateau (Feng et al. 2015) and $N\ (H_2) = 7.5 \times 10^{22}\,cm^{-2}$ for the extended ridge (Tercero et al. 2010). Table 3 summarizes the results for CP and CCP.

5. Discussion

(i) PO and PN in the Orion Plateau Outflow

The line profiles of PO and PN closely resemble each other, within the noise levels, with linewidths of 21–25 km s^{-1} and $V_{LSR} \sim 10$ km s^{-1} (see Figures 1 and 2; Table 1). These line parameters clearly associate PO and PN with the "plateau" outflow, also called the lower velocity flow, lying along the NE–SW axis in Orion-KL (e.g., Tercero et al. 2010; Feng et al. 2015). PO and PN therefore exist in the same gas and are likely to be chemically related. These two molecules are thought to be associated with each other in other molecular clouds, such as W51 1e/2e, W3(OH), or AFGL 5142 (Rivilla et al. 2016, 2020). In certain sources, however, the linewidths and LSR velocities may differ between PO and PN. In L1157, for example, the PN line profiles are broader by a factor of 2 than those of PO and are shifted in velocity by a few km s^{-1} (Lefloch et al. 2016). In our data, such differences are not apparent, within the uncertainties. There was also no evidence of the presence of either the ridge or "hot core" regions in the PO and PN spectra. The PN line parameters are identical to those originally observed by Ziurys (1987), who also suggested an origin in the plateau.

The column densities derived for PN and PO in the Orion-KL plateau are consistent with those obtained for these molecules in other dense molecular clouds with star formation, as shown in Table 2. For PN, $N_{tot} \approx 2.0 \pm 0.4 \times 10^{13}\,cm^{-2}$, lying within the range of values found for the other regions of 10^{11}–$2.1 \times 10^{13}\,cm^{-2}$. The column density in Orion is closest to that found in W51 1e/2e and the Galactic center cloud G + 0.693−0.03 (see Table 2). For PO in Orion, N_{tot} $5.4 \pm 0.2 \times 10^{13}\,cm^{-2}$, again within the range of values of other molecular clouds (10^{11}–$4 \times 10^{13}\,cm^{-2}$), and best matching those in W51 1e/2e and G + 0.693−0.03. The column densities in Orion are therefore among the largest known in star-forming clouds.

The fractional abundances derived for PO and PN in Orion are $f \sim 1.6(0.1) \times 10^{-10}$ and $6.1(0.6) \times 10^{-11}$, respectively,

Table 1
Observations of Phosphorus-bearing Molecules in Orion-KL

Molecule	Transition	Frequency (MHz)	T_A^*(mK)	V_{LSR} (km s^{-1})	$\Delta V_{1/2}$ (km s^{-1})
PO	$J = 2.5 \rightarrow 1.5$ $F = 3 \rightarrow 2$, e	108,998.45	16 ± 2	10.2 ± 2.8	25.2 ± 2.8
	$J = 2.5 \rightarrow 1.5$ $F = 2 \rightarrow 1$, e	109,045.40	10 ± 2	10.9 ± 2.7	21.6 ± 2.7
	$J = 2.5 \rightarrow 1.5$ $F = 3 \rightarrow 2$, f[a]	109,206.20	18 ± 2	10.0 ± 2.7	24.3 ± 2.7
	$J = 2.5 \rightarrow 1.5$ $F = 2 \rightarrow 1$, f[b]	109,281.19	11 ± 2	∼9	∼20
PN	$J = 2 \rightarrow 1$	93,979.77	19 ± 2	9.7 ± 3.2	22.4 ± 3.2
CP[c]	$N = 2 \rightarrow 1$ $J = 2.5 \rightarrow 1.5$	95710.2 95712.6	<10	⋯	⋯
CCP[c]	$J = 8.5 \rightarrow 7.5$, f	108179.1 108182.2	<12	⋯	⋯
^{30}SiO[d]	$J = 2 \rightarrow 1$	84746.2	140 ± 10	9 ± 4	21.5 ± 3.5
SiS	$J = 5 \rightarrow 4$	90771.6	35 ± 3	9.2 ± 3.3	20.1 ± 3.3
	$J = 6 \rightarrow 5$	108924.3	59 ± 2	9.8 ± 2.8	21.4 ± 2.8

Notes.
[a] Possible weak (<10%) contamination by $J_{Ka,Kc} = 16_{1,15} \rightarrow 15_{1,14}$ transition of ethyl formate.
[b] On shoulder of $N = 3 \rightarrow 2$, $J = 2 \rightarrow 1$ transition of SO.
[c] Two hyperfine components.
[d] Partially blended with $J\tau = 19_4 \rightarrow 18_5$ line of CH_3OH (see Ziurys 1988).

based on $N(H_2) = 3.3 \times 10^{23}$ cm^{-2} for the plateau (Feng et al. 2015). These abundances are similar for values found in the other clouds (∼10^{-11}–10^{-9}). They are not nearly as high as those found in L1157, which has $f(PO) \sim 10^{-8}$ and $f(PN) \sim 10^{-9}$. Because PO and PN arise from the same gas, their ratio supplies an important constraint. In Orion-KL, PO/PN ∼ 3—identical to that in W3(OH), B1 and L1157, and within a factor of 2 of W51 and G + 0.693−0.03. The consistency of the PO/PN among the sources is remarkable.

(ii) The Case for Shock Chemistry

The line profiles observed in both PO and PN are similar to those of SiO and SiS as mentioned (see Figures 2 and 3 and Table 1). The silicon species all have $\Delta V_{1/2} \sim$ 20–21 km s^{-1}, with V_{LSR} near 9–10 km s^{-1}, ignoring the high-velocity wings in SiO. Note that a transition of ^{30}SiO was chosen to avoid optical depth effects. However, ^{30}SiO also has the high-velocity line wings that trace the SE-NW outflow bright in vibrationally excited H_2, that lies roughly perpendicular to the plateau flow (e.g., Feng et al. 2015). The $J = 6 \rightarrow 5$ transition of SiS also has a higher intensity than expected, in comparison to the $J = 5 \rightarrow 4$ line, also noted by Ziurys (1988), suggestive of minor contamination (<25%).

Both SiO and SiS are thought to be formed almost exclusively in shocks toward star-forming regions (e.g., Ziurys 1987, 1988, 1991). Such "shock chemistry" may simply arise from grain destruction, which releases refractory elements such as silicon into the gas phase, and/or gas-phase reactions with barriers that can proceed at elevated temperatures (Ziurys 1988). While SiO may be produced directly by grain sputtering, SiS is more likely a result of gas-phase reactions with connections to shock outflows and grain destruction (e.g., Ziurys 1991; Podio et al. 2017). Based on ab initio calculations, Zanchet et al. (2018) found that an effective, gas-phase route to SiS is:

$$\mathrm{Si} + \mathrm{SO} \rightarrow \mathrm{SiS} + \mathrm{O}. \quad (1)$$

The rate constant for this process is $k_1 \sim 1.7 \times 10^{-11}$ cm^3 s^{-1} at $T \sim 125$ K, the estimated temperature of the plateau (Tercero et al. 2010). SO is very abundant in the Orion plateau, and grain sputtering in the shock could create atomic silicon, making this pathway very feasible. The reaction, however, also leads to SiO:

$$\mathrm{Si} + \mathrm{SO} \rightarrow \mathrm{SiO} + \mathrm{S}. \quad (2)$$

The rate constant here is $k_2 \sim 1.3 \times 10^{-10}$ cm^3 s^{-1} at $T \sim 125$ K—a factor of 7.5 faster. Hence, SiO is favored via this process, but SiS may still be produced.

Based on the results for SiO and SiS, PO and PN are also probably created in the shocked gas of the Orion plateau. The silicon-bearing species are known to be associated with shocks, as mentioned, and share similar line profiles to the phosphorus-containing molecules. Furthermore, Mininni et al. (2018) found a correlation of PN with SiO in star-forming regions, associating the P-bearing molecule with shocks, although a more limited number of regions showed evidence of a more quiescent formation pathway for PN. A likely scenario for PO and PN formation would first involve the liberation of phosphorus from the dust grains, followed by gas-phase reactions. PO and PN are unlikely to be directly evaporated from grain surfaces because neither molecule is found in the hot core. The carrier of phosphorus in the solid-state is uncertain. Jiménez-Serra et al. (2018) suggest that phosphorus is converted to phosphine, PH_3, as the grains are heated in the shock. Phosphine forms on the grain surface through hydrogenation before being nonthermally desorbed. The phosphine then evaporates and becomes available for additional gas-phase reactions. On the other hand, thermodynamics predicts that phosphorus is contained in phosphides, in particular, the P-metal alloy schreibersite, $(Fe,Ni)P_3$ (e.g., Pasek 2019). Predictions of the composition of grains formed around stars suggest all the phosphorus will be contained in schreibersite (Lodders & Fegley 1999: Lodders 2003), which, with a condensation temperature near ∼1250 K, could survive transport to molecular clouds. Therefore, phosphorus could be released from grains in some other form, such as

Table 2
Summary of PO and PN in Molecular Clouds

Source	Type	PN N_{tot} (cm^{-2})	PO N_{tot} (cm^{-2})	f(PN)	f(PO)	PO/PN	$\Delta V_{1/2}$ (km s^{-1})	Chemistry
AFGL 5142[a]	High-mass star formation	2.4×10^{12}[b]	4.9×10^{12}[b]	⋯	⋯	1.7[b]	1.0–5.0	Post-shock photochemistry
B-1[c]	Low-mass protostar	10^{11}–10^{13}[d]	10^{12}–10^{13}[d]	10^{-10}–10^{-9}[d]	10^{-10}–10^{-9}[d]	1–3[d]	1–2	Shock formation
G + 0.693−0.03[e]	High-mass star formation	5.6×10^{12}	8×10^{12}	⋯	⋯	1.5	17–24	Shock formation
L1157[f]	Low-mass star formation	9×10^{11}	2×10^{12}	0.9×10^{-9}	2.5×10^{-9}	3	10–20	Shock formation
W51 e1/e2[g]	High-mass star formation	2.1×10^{13}	4×10^{13}	10^{-10}	2×10^{-10}	1.8	7.0–8.2	Ion–molecule/ Freeze out/ Evaporation
W3(OH)[g]	High-mass star formation	2×10^{12}	6×10^{12}	4×10^{-11}	1.2×10^{-10}	3	6.6	Ion–molecule/ Freeze out/ Evaporation
Orion-KL[h]	High-mass star formation	$2.0(0.4) \times 10^{13}$	$5.4(0.2) \times 10^{13}$	$6.1(0.6) \times 10^{-11}$	$1.6(0.1) \times 10^{-10}$	2.7	20–25	Shock formation

Notes.
[a] Rivilla et al. (2020).
[b] Average over multiple positions and velocity components.
[c] Bergner et al. (2019).
[d] Range reflects source size variation.
[e] Rivilla et al. (2018).
[f] Lefloch et al. (2016).
[g] Rivilla et al. (2016).
[h] This work.

Table 3
Upper Limits to the Abundances of CP and CCP in Orion-KL

Molecule	Component	N_{tot} (cm^{-2})	f (X/H_2)
CCP[a]	Plateau	$<6.5 \times 10^{12}$	$<2.0 \times 10^{-11}$
	Extended ridge	$<2.2 \times 10^{11}$	$<2.9 \times 10^{-12}$
CP[a]	Plateau[b]	$<4.5–5.3 \times 10^{13}$	$<1.4–2.3 \times 10^{-10}$
	Extended ridge	$<1.3 \times 10^{12}$	$<1.7 \times 10^{-11}$

Notes.
[a] Hyperfine components assumed collapsed for analysis.
[b] Range reflects RADEX and analytical calculation.

iron-phosphorus or nickel-phosphorus species. Based on condensation temperatures, if silicates are destroyed in the shock, it is likely schreibersite is as well. The condensation temperature of common silicates is near 1300 K (Lodders & Fegley 1999; Lodders 2003).

Once phosphorus is in the gas phase, PO could be formed from destruction products of PH_3 (Jiménez-Serra et al. 2018), such as:

$$PH_2 + O \rightarrow PO + H_2 \quad (3)$$

$$PH + O \rightarrow PO + H. \quad (4)$$

Here rate constants are $k_3 \sim 4 \times 10^{-11}\,cm^3\ s^{-1}$ and $k_4 \sim 10^{-10}\,cm^3\,s^{-1}$, respectively, with no temperature dependence (e.g., McElroy et al. 2012). Other routes may be possible, for example, NiP + O, but reaction rates are not known. The synthesis of PN is thought to be linked to that of nitrogen and PO, via the processes (Jiménez-Serra et al. 2018):

$$PO + N \rightarrow PN + O \quad (5)$$

$$PH + N \rightarrow PN + H. \quad (6)$$

The rate constant for reaction (5) has an inverse temperature dependence, such that it increases as $T \rightarrow 0$ K. At 125 K, the value is $k_5 \sim 5 \times 10^{-11}\,cm^3\ s^{-1}$—comparable to that of reaction (6). Another route to PN could be the reaction of N + CP with $k \sim 3 \times 10^{-10}\,cm^3\,s^{-1}$ (e.g., Chantzos et al. 2020); this rate of this process is relatively fast and is consistent with the lack of phosphorus carbide in Orion (see Table 3). Given their respective rates, PH is more likely to react with O than N, leading to PO. Then PN is formed from PO, linking the chemistry of these two molecules.

Jiménez-Serra et al. (2018) examined the formation of PO and PN in C-type shocks with $v_{shock} \sim 20–40\,km\,s^{-1}$, applicable to the Orion plateau region. They consistently calculated PN > PO, unless they considered the reaction:

$$P + OH \rightarrow PO + H. \quad (7)$$

The adopted rate constant for this process at 125 K is $k_7 \sim 6.6 \times 10^{-11}\,cm^3\ s^{-1}$, making it comparable to reactions (3) and (4). However, the reaction may have a barrier that requires elevated temperatures in order to become efficient. Because we observe $PO/PN \sim 3$, this pathway may be important in Orion. The introduction of cosmic rays could also flip the PO/PN ratio if reaction (7) is not considered (Jiménez-Serra et al. 2018). However, the Orion plateau outflow, to our knowledge, is not a significant source of cosmic rays.

CP and CCP were not detected in the Orion plateau, with upper limits to the fractional abundances of $f(CP/H_2) < 2 \times 10^{-10}$ and $f(CCP/H_2) < 2 \times 10^{-11}$. These upper limits are close to the abundances derived for PO and PN. These results are qualitatively consistent with shock destruction of grains, which releases excess oxygen from silicates, along with phosphorus. The oxygen then reacts with P to create PO. If carbon is also released from grains, and CP is formed, it is quickly converted to PO, as previously discussed.

(iii) Toward a Unified Picture of the Chemical Formation of PO and PN

As shown in Table 2, PO and PN in other molecular clouds arise from (1) chemistry associated with shocks, as traced by SiO (B1, L1157, G+0.693−0.03); (2) formation by cold, ion–molecule and neutral–neutral reactions, followed by grain condensation and then evaporation (W51, W3(OH)); or (3) post-shock photochemistry (AFGL 5142). It can be argued that the unique geometry of AFGL 5142 makes it a special case for photochemistry. The two formation routes remaining appear to be at odds: quiescent versus high temperature shock-related pathways.

As mentioned, Orion-KL is a nearby, well-studied region with distinct velocity components that serve as useful chemical benchmarks. In this source, PO and PN do not appear to arise from either the hot core or the extended ridge components. Absence in the hot core suggests that PO and PN in Orion are not a result of direct evaporation from grains, as suggested for W51 and W3(OH). Upper limits in the hot core, assuming a 10″ source size, are $f(PO/H_2) \sim 2 \times 10^{-11}$ and $f(PN/H_2) \sim 4 \times 10^{-11}$, if $N(H_2) \sim 10^{24}\,cm^{-2}$ (Feng et al. 2015)—less than the abundances found in the plateau (see Table 2). Furthermore, the lack of a ridge component in these two molecules indicates that cold, quiescent, ion–molecule-type chemistry is also not an effective synthesis route.

The PO/PN ratios in W51 and W3(OH) fall in the range of those measured in the clouds where shock formation is occurring (PO/PN ∼ 1–3), and the abundances are very similar (see Table 2). Furthermore, the line widths of the two phosphorus molecules in both sources are not particularly narrow, with $\Delta V_{1/2} \sim 6–8\,km\,s^{-1}$ (Rivilla et al. 2016). These observational facts suggest that perhaps PO and PN in W51 and W3(OH) are also formed in shocked material, by the processes described. The sequence leading to the formation of PO and PN in W51 and W3(OH) of quiescent, colder chemistry, followed by grain condensation and subsequent evaporation, is complex, with many free parameters, as well as numerous unknowns. Quiescent chemistry and grain evaporation do not appear to play an important role for phosphorus in Orion; not only are PO and PN absent from the ridge, but CCP and CP are as well, with upper limits of $f < 3 \times 10^{-12}$ and 2×10^{-11}, respectively (see Table 3). Furthermore, neither PN nor PO have been found in very cold, dark clouds since the searches of Turner et al. (1990). Clearly further studies of PO and PN in molecular clouds are needed to fully understand the nature of their interstellar synthesis.

6. Conclusions

This study presents yet another detection of PO in star-forming regions, following the pioneering works of others (e.g., Lefloch et al. 2016; Rivilla et al. 2016; Bergner et al. 2019). It appears that PO is fairly common in high-mass star-forming regions, and perhaps in low mass sources as well, as further

studies may reveal. As in other clouds, in the Orion-KL region, PO is clearly associated with PN, suggesting the two molecules are formed in concert through related reactions. One possible scenario is destruction of schreibersite grains, followed by gas-phase reactions. PO is formed first, which then reacts to create PN. Searches for additional phosphorus-containing species such as PH, PH_2, and PH_3 would help elucidate the phosphorus chemical network in star-forming clouds.

This work was supported by NASA grant 80NSSC18K0584 (Emerging Worlds), NSF grant AST-1907910, NIH grant R25GM062584, and the Sloan Foundation Baseline Scholars Program. The authors thank Dr. Deborah Schmidt for use of the reduced chi-square program.

ORCID iDs

J. J. Bernal https://orcid.org/0000-0001-6176-0773
L. M. Ziurys https://orcid.org/0000-0002-1805-3886

References

Agúndez, M., Cernicharo, J., Decin, L., Encrenaz, P., & Teyssier, D. 2014, ApJL, 790, L27
Agúndez, M., Cernicharo, J., & Guélin, M. J. 2007, ApJL, 662, L91
Agúndez, M., Cernicharo, J., Pardo, J. R., Guélin, M., & Phillips, T. G. 2008, A&A, 485, L33
Altwegg, K., Balsiger, H., Bar-Nun, A., et al. 2016, SciA, 2, 1600285
Barnes, J. J., Tartèse, R., Anand, M., et al. 2014, E&PSL, 390, 244
Bergner, J. B., Öberg, K. I., Walker, S., et al. 2019, ApJL, 844, L36
Chantzos, J., Rivilla, V. M., Vasyunin, A., et al. 2020, A&A, 633, A54
de Beck, E., Kamiński, T., Patel, N. A., et al. 2013, A&A, 558, A132
Dubernet, M.-L., Alexander, M. H., Ba, Y. A., et al. 2013, A&A, 553, A50
Feng, S., Beuther, H., Henning, T., et al. 2015, A&A, 581, A71
Fletcher, L. N., Orton, G. S., Teanby, N. A., & Irwin, P. G. J. 2009, Icar, 202, 543
Fontani, F., Rivilla, V. M., Caselli, P., Vasyunin, A., & Palau, A. 2016, ApJL, 822, L30
Freund, R. W., Ziurys, L. M., Reiland, G. P., & Lauria, E. F. 2011, in 30th URSI General Assembly and Scientific Symposium (Piscataway, NJ: IEEE), 1
Guélin, M., Cernicharo, J., Paubert, G., & Turner, B. E. 1990, A&A, 230, L9
Halfen, D. T., Clouthier, D. J., & Ziurys, L. M. 2008, ApJL, 677, L101
Harayama, T., & Riezman, H. 2018, Nat. Rev. Mol. Cell Biol., 19, 281
Hirota, T., Bushimata, T., Choi, Y. K., et al. 2007, PASJ, 59, 897
Hughes, J. M., & Rakovan, J. 2002, RvMG, 48, 1
Jacobsen, H. R., Thanathibodee, T., Frebel, A., et al. 2014, ApJL, 796, L24
Jiménez-Serra, I., Viti, S., Quènard, D., & Holdship, J. 2018, ApJ, 862, 128
Koo, B.-C., Lee, Y.-H., Moon, D.-S., Yoon, S.-C., & Raymond, J. C. 2013, Sci, 342, 1346
Lebouteiller, V., Kuassivi, V., & Ferlet, R. 2006, in ASP Conf. Ser. 348, Astrophysics in the far Ultraviolet: Five Years of Discovery with FUSE, ed. G. Sonneborn, H. W. Moos, & B.-G. Anderson (Victoria, BC: ASP), 480
Lefloch, B., Vastel, C., Viti, S., et al. 2016, MNRAS, 462, 3937
Lodders, K. 2003, ApJ, 591, 1220
Lodders, K., & Fegley, B., Jr. 1999, in IAU Symp. 191, Asymptotic Giant Branch Stars, ed. T. Le Bertre, A. Lèbre, & C. Waelkens (San Francisco, CA: ASP), 279
Maciá, E. 2005, Chem. Soc. Rev., 34, 691
McElroy, D., Walsh, C., Markwick, A. J., et al. 2012, A&A, 550, A36
Milam, S. N., Halfen, D. T., Tenenbaum, E. D., et al. 2008, ApJ, 684, 618
Mininni, C., Fontani, F., Rivilla, V. M., et al. 2018, MNRAS, 476, L39
Pasek, M. A. 2019, Icar, 317, 59
Podio, L., Codella, C., Lefloch, B., et al. 2017, MNRAS, 470, L16
Rivilla, V. M., Drozdovskaya, M. N., Altwegg, K., et al. 2020, MNRAS, 492, 1180
Rivilla, V. M., Fontani, F., Beltrán, M. T., et al. 2016, ApJ, 826, 161
Rivilla, V. M., Jiménez-Serra, I., Zeng, S., et al. 2018, MNRAS, 475, L30
Schöier, F. L., van der Tak, F. F. S., van Dishoeck, E. F., & Black, J. H. 2005, A&A, 432, 369
Tenenbaum, E. D., Woolf, N. J., & Ziurys, L. M. 2007, ApJL, 666, L29
Tenenbaum, E. D., & Ziurys, L. M. 2008, ApJL, 680, L121
Tercero, B., Cernicharo, J., Pardo, J. R., & Goicoechea, J. R. 2010, A&A, 517, A96
Tercero, B., Vincent, L., Cernicharo, J., Viti, S., & Marcelino, N. 2011, A&A, 528, A26
Turner, B. E., Tsuji, T., Bally, J., Guelin, M., & Cernicharo, J. 1990, ApJ, 365, 569
van der Tak, F. F. S., Black, J. H., Schöier, F. L., Jansen, D. J., & van Dishoeck, E. F. 2007, A&A, 468, 627
Zanchet, A., Roncero, O., Agúndez, M., & Cernicharo, J. 2018, ApJ, 862, 38
Ziurys, L. M. 1987, ApJL, 321, L81
Ziurys, L. M. 1988, ApJ, 324, 544
Ziurys, L. M. 1991, ApJ, 379, 260
Ziurys, L. M., Schmidt, D. R., & Bernal, J. J. 2018, ApJ, 856, 169